

# The origin and tidal evolution of cuspy triaxial haloes

Ben Moore <sup>\*</sup>, Stelios Kazantzidis, Jürg Diemand and Joachim Stadel

*Institute for Theoretical Physics, University of Zürich, CH-8057 Zürich, Switzerland*

1 November 2018

## ABSTRACT

We present a technique for constructing equilibrium triaxial  $N$ -body haloes with nearly arbitrary density profiles, axial ratios and spin parameters. The method is based on the way in which structures form in hierarchical cosmological simulations, where prolate and oblate haloes form via mergers with low and high angular momentum, respectively. We show that major mergers between equilibrium spherical cuspy haloes produce similarly cuspy triaxial remnants and higher angular-momentum mergers produce systems with lower concentrations. Triaxial haloes orbiting within deeper potentials become more spherical and their velocity dispersion tensors more isotropic. The rate of mass loss depends sensitively on the halo shape: a prolate halo can lose mass at a rate several times higher than an isotropic spherical halo with the same density profile. Subhaloes within cosmological simulations are significantly rounder than field haloes with axial ratios that are  $\sim 30\%$  larger.

**Key words:** methods:  $N$ -body simulations – galaxies: haloes – galaxies: interactions – cosmology: theory – dark matter.

## 1 INTRODUCTION

A generic prediction of the currently favoured cold dark matter (CDM) cosmological model of hierarchical structure formation is that dark matter (DM) haloes of galaxies and clusters are flattened triaxial systems (e.g., Barnes & Efstathiou 1987; Frenk et al. 1988; Dubinski & Carlberg 1991; Warren et al. 1992; Cole & Lacey 1996; Thomas et al. 1998; Jing & Suto 2002). Observationally, inferring the intrinsic shape of DM haloes of galaxies and clusters is a difficult task, but nonetheless several potentially powerful probes exist that may allow us to distinguish between spherical and flattened DM haloes. These include the dynamical modelling of collisionless tracers such as tidal streams orbiting the Milky Way (Johnston et al. 1999; Ibata et al. 2001; Mayer et al. 2002; Majewski et al. 2004), the distribution and kinematics of gas in spiral galaxies (Kuijken & Tremaine 1994; Franx, van Gorkom & de Zeeuw 1994; Schoenmakers, Franx & de Zeeuw 1997; Merrifield 2002), and polar ring galaxies (Schweizer, Whitmore & Rubin 1983; Sackett & Sparke 1990; Sparke 2002; Iodice et al. 2003) which provide shape constraints perpendicular to the disc plane, gravitational lensing applications (Kochanek 1995; Bartelmann, Steinmetz & Weiss 1995; Koopmans et al. 1998; Oguri, Lee & Suto 2003) and the flattening of the extended X-ray isophotes in elliptical galaxies (Buote & Canizares 1994, 1996, 1998; Buote et al. 2002).

Numerical experiments of isolated equilibrium models are very useful for studying the dynamical evolution of gravitat-

ing systems in a controlled way. Several techniques exist for constructing  $N$ -body realizations of spherical haloes and multi-component galaxies (Hernquist 1993; Holley-Bockelmann et al. 2003; Kazantzidis, Magorrian & Moore 2004a, hereafter KMM), but it is far more complicated to build triaxial equilibria. Even though the Jeans theorem guarantees that the distribution function depends only on the isolating integrals of motion, explicit expressions for the latter other than the energy per unit mass,  $E$ , are rarely known in the case of triaxial potentials. As a result, the triaxial models that have been constructed so far have been either limited to a few special analytical cases (e.g., Stäckel potentials or rotating  $f(E_J)$  models with  $E_J$  being the Jacobi constant) or entirely based on numerical techniques (Schwarzschild 1979, 1993; Merritt & Fridman 1996; Poon & Merritt 2001; Terzić 2003).

Recently, Holley-Bockelmann et al. (2001) used a technique of adiabatically applying a drag to the velocities of the particles along each principal axis in order to create cuspy triaxial systems starting with a spherical Hernquist (Hernquist 1990) model. The original prescription of Hernquist (1993) was generalized by Boily, Kroupa & Peñarrubia-Garrido (2001) for accommodating composite, axisymmetric models of galaxies and extended by Tinker & Ryden (2002) for investigating the effect of rotating, triaxial halos on disk galaxies. These techniques are useful and have been used to understand the response of systems to live triaxial potentials. However, they are somewhat restricted to modest values of the flattening and it is difficult to incorporate a significant amount of rotational flattening.

Triaxiality can arise in a number of ways. The most common way of constructing numerical models of triaxial galaxies is via the merger of other objects. Examples include binary mergers of spherical haloes (e.g., White 1978; Fulton & Barnes 2001) and disk

<sup>\*</sup> E-mail: moore@physik.unizh.ch (BM); stelios@physik.unizh.ch (SK); diemand@physik.unizh.ch (JD), stadel@physik.unizh.ch (JS)

galaxies (e.g., Gerhard 1981; Barnes 1992; Barnes & Hernquist 1996; Naab & Burkert 2003; Kazantzidis et al. 2004b), as well as multiple mergers of systems (e.g., Weil & Hernquist 1996; Dubinski 1998). The structure of the final remnant of two component models depends sensitively on both the orbital geometry (Naab & Burkert 2003) as well as on the inclination and internal properties of the disks (Kazantzidis et al. 2004b).

A general technique for constructing cuspy axisymmetric and triaxial  $N$ -body systems would be advantageous for many purposes including studying the dynamical friction in flattened and rotating systems, the mass loss and tidal stripping from triaxial substructure haloes, the effects of baryonic accretion and disc formation on triaxial halo shape and anisotropy, the effects of triaxial shape on the properties and stability of discs, the interaction between central black holes and cusps and the inflow of gas in triaxial systems.

In this paper we explore the generation of triaxial structures that is based on the way that haloes in hierarchical models of structure formation obtain their shapes. Inspection of a cosmological simulation reveals that triaxiality arises via mergers that take place with various amounts of angular momentum which is generated from the large-scale tidal field. Mergers between two haloes that occur with little angular momentum (radial mergers) produce prolate systems, whilst high angular momentum mergers produce oblate systems. Most CDM haloes form via a sequence of mergers with varying amounts of angular momentum such that haloes with arbitrary triaxiality may be formed and the triaxiality will vary with radius (Moore et al. 2001; Vitvitska et al. 2002).

The outline of this paper is as follows. In Section 2, we describe our technique for constructing equilibrium cuspy  $N$ -body haloes with various degrees of flattening. There we discuss in detail the numerical experiments we performed and present our results for the internal structure of the resulting models. In Section 3, we investigate the tidal evolution of triaxial substructure haloes within a static host potential and study the shape of subhaloes within a cosmological CDM simulation. Finally, we summarise our main results in Section 4.

## 2 CONSTRUCTING CUSPY TRIAXIAL DARK MATTER HALOES

We begin with a cuspy spherical DM halo which follows the Navarro, Frenk & White (1996, hereafter NFW) density profile

$$\rho(r) = \frac{\rho_s}{(r/r_s)(1+r/r_s)^2} \quad (r \leq r_{\text{vir}}). \quad (1)$$

Here the characteristic inner density  $\rho_s$  and scale radius  $r_s$ , are sensitive to the epoch of halo formation and tightly correlated with the halo virial parameters, via the concentration,  $c$ , and the virial overdensity  $\Delta_{\text{vir}}$ . Since the NFW density profile corresponds to a cumulative mass distribution that diverges as  $r \rightarrow \infty$ , we implement an exponential cut-off for  $r > r_{\text{vir}}$  which sets in at the virial radius and turns off the profile on a scale  $r_{\text{decay}}$  which is a free parameter and controls the sharpness of the transition

$$\rho(r) = \frac{\rho_s}{c(1+c)^2} \left(\frac{r}{r_{\text{vir}}}\right)^\epsilon \exp\left[-\frac{r-r_{\text{vir}}}{r_{\text{decay}}}\right] \quad (r > r_{\text{vir}}), \quad (2)$$

where  $c \equiv r_{\text{vir}}/r_s$  is the concentration parameter. Finally, in order to ensure a smooth transition between (1) and (2) at  $r_{\text{vir}}$ , we require the logarithmic slope there to be continuous. This implies

$$\epsilon = -\frac{1+3c}{1+c} + \frac{r_{\text{vir}}}{r_{\text{decay}}}. \quad (3)$$

Once the density profile  $\rho(r)$  of our initial model has been specified, we construct an  $N$ -body realization using the technique discussed in detail in KMM. To summarize, the particle positions and velocities are initialized by sampling the exact phase-space distribution function using Eddington's inversion formula (Eddington 1916) for the given density profile  $\rho(r)$  and assuming spherical symmetry. Note that in this paper we will consider only initial models with isotropic velocity dispersion tensors and therefore their distribution function will only depend on the binding energy  $E$ ,  $f = f(E)$ . For the following experiments we begin with an initial galaxy-sized halo with virial mass  $M_{\text{vir}} = 7 \times 10^{11} h^{-1} M_\odot$  and concentration of  $c = 10$  in accordance with theoretical predictions for objects at this mass scale and for the adopted cosmology (e.g., Bullock et al. 2001). Note that for all simulations presented in this paper including the cosmological ones described in the next section, we consider as our framework the concordance flat  $\Lambda$ CDM model with present-day matter and vacuum densities  $\Omega_m = 0.3$  and  $\Omega_\Lambda = 0.7$ , respectively, dimensionless Hubble constant  $h = 0.7$ , present-day fluctuation amplitude  $\sigma_8 = 0.9$  and index of the primordial power spectrum  $n = 1.0$ . For this choice of concentration, the virial and scale radius of the initial halo model are  $r_{\text{vir}} = 181 h^{-1} \text{ kpc}$  and  $r_s = 18.1 h^{-1} \text{ kpc}$ , respectively. The initial model is constructed with  $N = 5 \times 10^5$  particles and we use a gravitational softening of  $\epsilon = 0.3 h^{-1} \text{ kpc}$ .

All the simulations presented in this paper were carried out using PKDGRAV, a multi-stepping, parallel  $N$ -body code (Stadel 2001) which uses a spline kernel softening and multi-stepping based on the local acceleration of particles. The time integration was performed with high enough accuracy such that the total energy was conserved to better than 0.1% in all cases. We have also explicitly checked that our results are not compromised by choices of force softening, time-stepping or opening angle criteria in the treecode.

We perform a first experiment in which we merge two identical spherical haloes with zero angular momentum corresponding to a head-on collision with an impact parameter  $b = 0$ . The initial relative separation of the two haloes is  $r_{\text{sep}} = 210 h^{-1} \text{ kpc}$  and are they infalling at a relative speed of  $v_{\text{rel}} = 300 \text{ km s}^{-1}$ . Relative velocities significantly higher than this value lead to unbound orbits, so we chose this value so as to maximize the amount of flattening from a single merger. Note that the initial separation corresponds to haloes which are overlapping. This does not influence the final result as nearly identical remnants were produced with non-overlapping initial models. The two haloes merge within a time-scale of order the crossing time  $t_{\text{cross}} = \sqrt{r_{\text{vir}}^3/GM_{\text{vir}}}$  which is approximately equal to 2 Gyr for our initial models. In all simulations the merger remnants were allowed to settle into equilibrium for several crossing times after the merger was complete which was established by monitoring the fluctuations of the density profile of the final system. In addition, the virial ratio  $2T/W$  varied between 0.1 and 0.3% from 1.0 for the same time-scales confirming that our triaxial remnants are indeed in equilibrium. In all cases the centre of the remnant is identified using the most bound particle, which agrees very well with the centre of mass recursively calculated using smaller spherical regions.

The radial merger produces a prolate axisymmetric system with axial ratios  $a:b:c = 2:1:1$  where  $a$ ,  $b$  and  $c$  are the long, intermediate and short axis, respectively. For each remnant, we calculate principle axis ratios  $s = b/a$  and  $q = c/a$  ( $a > b > c$ ), from the eigenvalues of a modified dimensionless inertia tensor (e.g., Dubinski & Carlberg 1991):  $I_{ij} = \sum x_i x_j / q^2$ , where  $q^2 = x^2 + (y/s)^2 + (z/q)^2$  is the ellipsoidal coordinate. We use an iter-

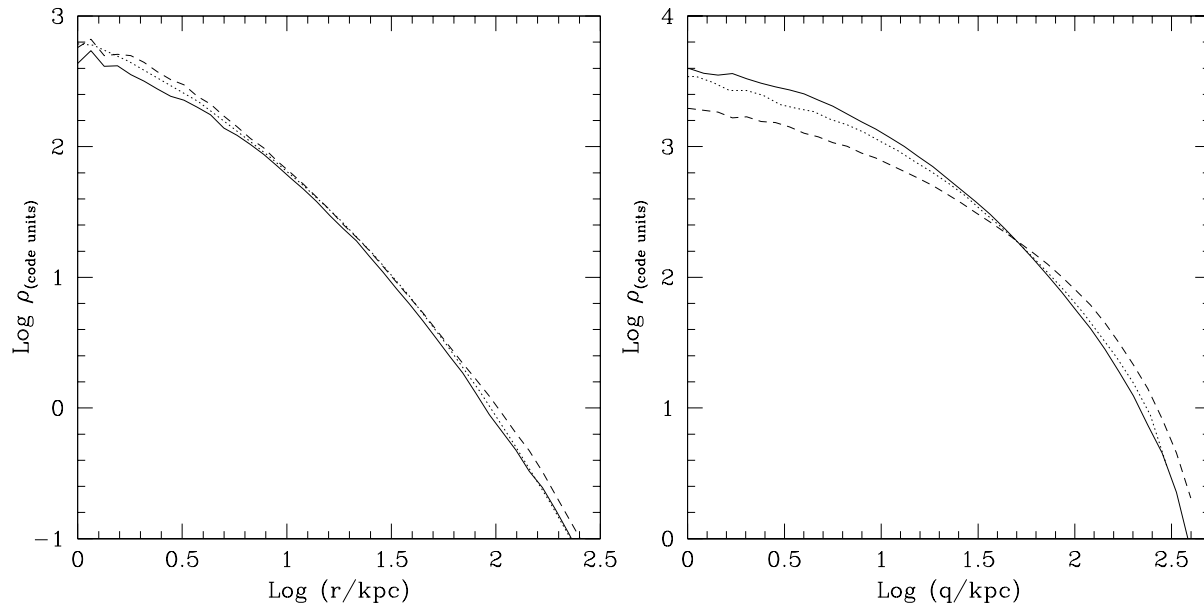


**Figure 1.** Density profiles of the initial model (dotted curve), the  $a:b:c = 2:1:1$  prolate model (solid curve) and the  $a:b:c = 2:2:1$  oblate model (dashed curve). The density was calculated using spherically averaged (left panel) and ellipsoidally averaged (right panel) bins such that the density is projected onto the symmetry axis.

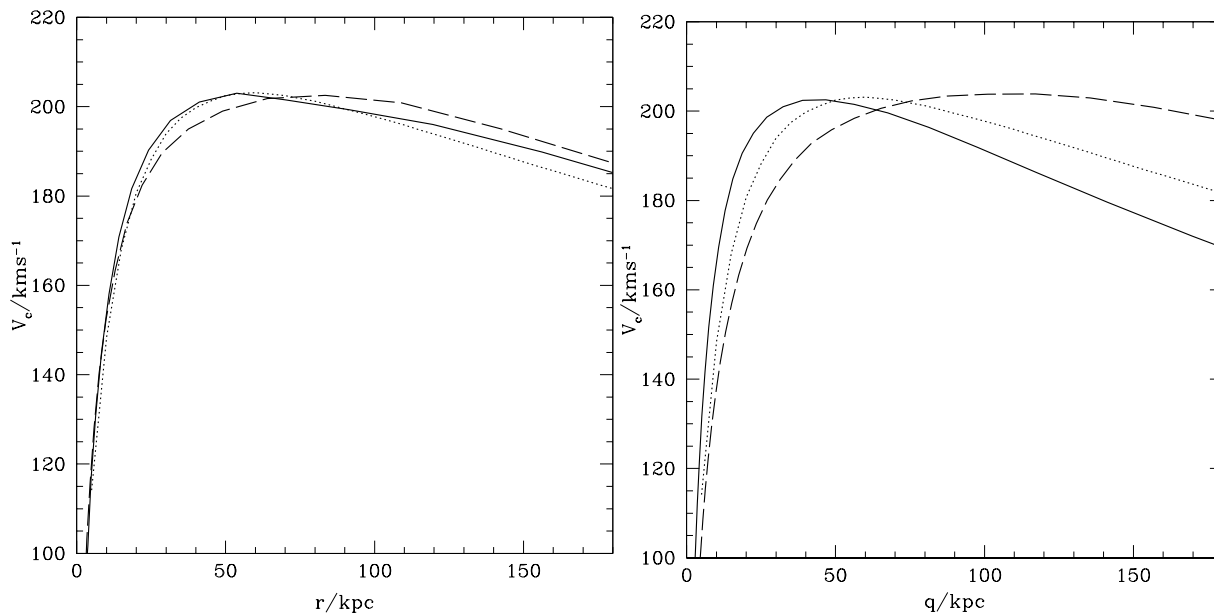


**Figure 2.** Circular velocity curves scaled to the same peak circular velocity for the initial model (dotted curve), prolate  $a:b:c = 2:1:1$  halo (solid curve) and oblate  $a:b:c = 2:2:1$  halo (dashed curve). The mass distribution was calculated using spherically averaged (left panel) and ellipsoidally averaged (right panel) bins. In each case the circular velocities are scaled to the same peak velocity assuming  $V_c \propto r$ .

ative algorithm starting with a spherical configuration ( $a = b = c$ ), and use the results of the previous iteration to define the principle axes of the next iteration. The procedure is iterated until the values of both axial ratios  $b/a$  and  $c/a$  have a percentage change of less than  $10^{-3}$ . The dimensionless spin parameter of this remnant, which is defined by

$$\lambda = \frac{J|E|^{1/2}}{GM^{5/2}} \quad (4)$$

where  $J$ ,  $E$  and  $M$  are the total angular momentum, binding energy and mass respectively, corresponds to  $\lambda = 0$  as expected in a radial merger.

In a second experiment we start with the two spherical haloes separated again by  $r_{\text{sep}} = 210h^{-1}$  kpc, but we give one halo a transverse velocity equal to the circular velocity of the combined model at that distance,  $v_{\text{rel}} = 240 \text{ km s}^{-1}$ . The circular orbit merger produces an oblate halo with axial ratios  $a:b:c = 2:2:1$ . As we demonstrate later (see Figure 4), haloes with any amount of triaxiality between these values could be created by using unequal-

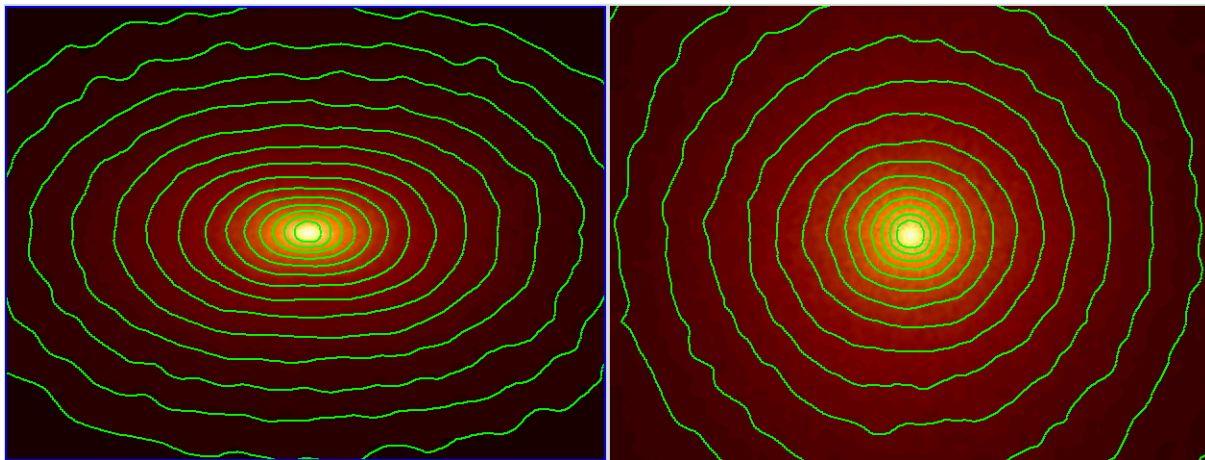


**Figure 3.** Logarithmically spaced surface density contours of the oblate model viewed in the plane of the long axis (left) and short axis (right).

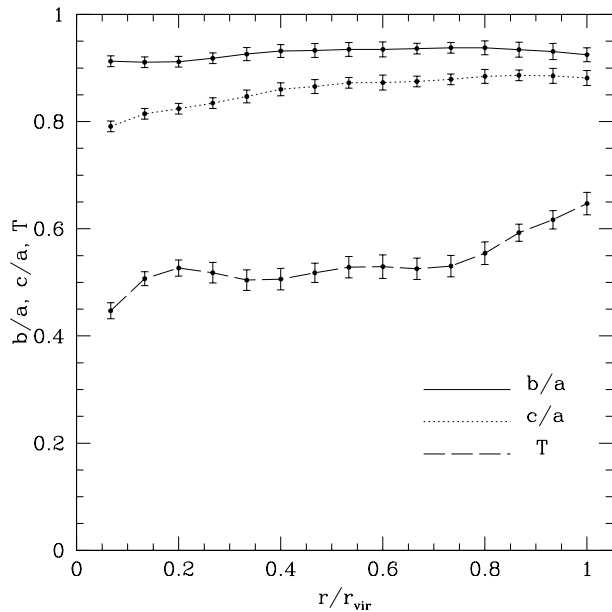


**Figure 4.** Axial ratios and triaxiality parameter of the minor merger remnant. The solid, dotted and dashed lines, respectively, show results for  $b/a$ ,  $c/a$  and  $T$ . The profile of the triaxiality parameter shows that this remnant is strongly triaxial with  $T \sim 0.5$ . The error bars represent the *rms* variation in the measurements from 20 time intervals spanning 10 half-mass dynamical times of the remnant at the end of the simulation. The errors in the axial ratios and triaxiality parameter are small demonstrating that the remnant is in equilibrium. We define the virial radius of the remnant,  $r_{\text{vir}}$ , to be the distance from the centre where the mean enclosed density is  $\sim 337$  times the mean universal density.

mass mergers or mergers with less or more angular momentum. The spin parameter of the final system is  $\lambda = 0.1$ . As expected, with these experiments we have been able to reproduce most of the range in  $\lambda$  seen in cosmological  $N$ -body simulations (e.g., Warren et al. 1992; Lemson & Kauffmann 1999). Although the formation histories of halos with a hierarchical universe is significantly more complex than these binary mergers, we might expect that oblate halos have a higher spin parameter and more angular momentum than prolate halos. Figure 1 shows the density profiles of the initial spherical model and that of the prolate and oblate haloes. The

panel on the left shows results using spherically-averaged bins. The density profiles on the right panel were calculated as a function of the ellipsoidal coordinate  $q$ , where  $q^2 = x^2 + (y/b)^2 + (z/c)^2$ . In agreement with other studies (e.g., White 1978; Villumsen 1983; Barnes 1999; Fulton & Barnes 2001; Boylan-Kolchin & Ma 2003), remnant central density slopes remain unchanged. In Figure 2 we show the circular velocity curves of the initial model and the final prolate and oblate haloes using again spherically averaged (left panel) and ellipsoidally averaged (right panel) bins. These have all been scaled by the same factor in radius and velocity such that all the curves have the same peak circular velocity. The prolate halo has a nearly identical concentration to the initial spherical model, but the oblate halo is nearly a factor of two less concentrated.

In order to create haloes with higher amounts of flattening it is necessary to merge together the products of the first set of simulations. Merging two prolate haloes along the long axis again at a velocity such that the system is just bound produces a  $a:b:c = 3:1:1$  remnant, while merging two oblate haloes in the plane of the long axis, but counter-rotating, results in a further flattened system with axial ratios  $a:b:c = 3:3:1$  and no net angular momentum, but with particles streaming in opposite directions. Figure 3 shows two contoured images of the oblate halo viewed projected along the short and long axis, respectively.

Finally, we performed a minor merger between two spherical halos with mass ratio equal to 4 : 1. The most massive halo was identical to the ones used in the previous experiments while the concentration of the smaller one was scaled according to Bullock et al. (2001) for the adopted  $\Lambda$ CDM cosmology. The orbital angular momentum of the merger was typical of cosmological encounters (Khojfar & Burkert 2003). The number of particles and gravitational softening used for the less massive halo was such that both halos were resolved with the same mass and force resolution. This is useful in the interpretation of the results regarding the structure of the remnant. Kazantzidis et al. (2004b) examined the evolution of disk galaxy merger remnants and found that their shapes evolve in the outer regions for several crossing times. In Figure 4, we demonstrate the stability of this remnant by running the simulation for a further 10 half-mass dynamical times and calculated profiles of axial ratios and triaxiality parameter [ $T \equiv (a^2 - b^2)/(a^2 - c^2)$ ] at 20 intermediate steps. The error bars in Figure 4 show the *rms* variation in the profiles at each radius and demonstrate that the remnant is in equilibrium.

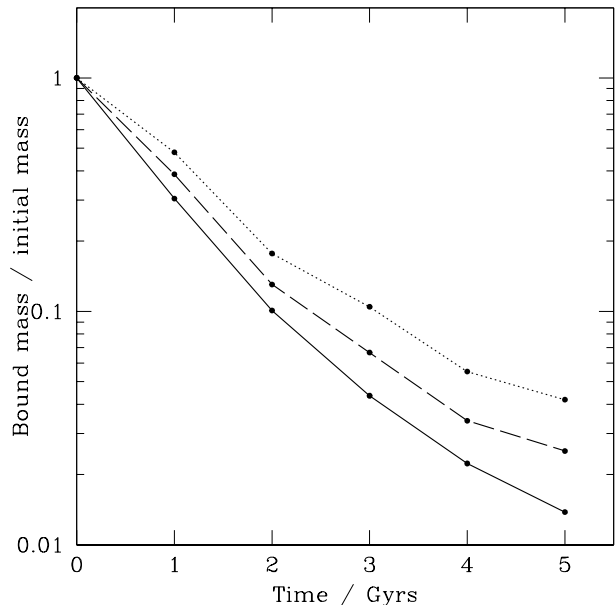


**Figure 5.** The rate of tidal mass loss over a period of 5 Gyrs ( $\sim 2$  orbital periods) for the initial spherical model (dotted line), the  $a:b:c = 3:1:1$  prolate model (solid curve) and the  $a:b:c = 3:3:1$  oblate model (dashed curve). The prolate halo experiences much more efficient tidal stripping than both the spherical and oblate halo on the same external tidal field and orbit which is probably caused by the orbital distribution of particles supporting its shape.

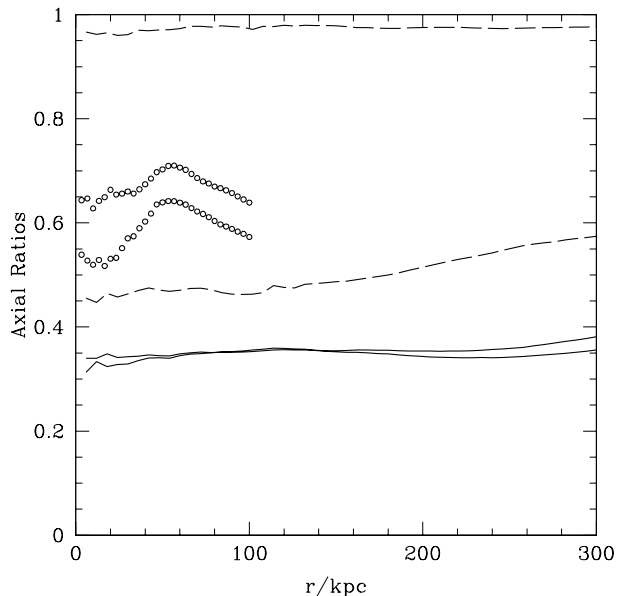


**Figure 6.** The axial ratios as a function of radius for the prolate (solid lines) and oblate (dashed lines) 3:1 haloes. The open circles show the axial ratios of the same prolate model after orbiting for 5 Gyrs within a deeper potential.

### 3 TIDAL EVOLUTION OF TRIAXIAL SUBHALOES

Numerical investigations of the tidal stripping and mass loss of substructure haloes in CDM models have previously been restricted to spherical systems with isotropic velocity dispersion tensors (e.g., Taffoni et al. 2003; Hayashi et al. 2003). The results of these simulations are also incorporated into semi-analytic mod-

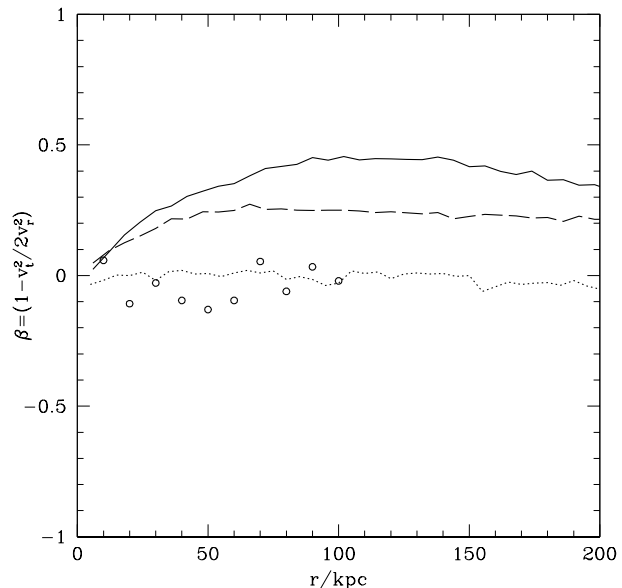


**Figure 7.** The anisotropy parameter  $\beta$  as a function of radius for the prolate halo model (solid line), oblate halo (dashed line) and initial conditions (isotropic spherical halo, dotted line). The open symbols show the anisotropy parameter for the prolate halo after orbiting for 5 Gyrs within a deeper potential.

els which attempt to follow the tidal evolution of orbiting subhaloes. However, the shapes and velocity dispersion tensors of haloes in cosmological simulations have been studied by many authors (e.g., Warren et al. 1992; Cole & Lacey 1996; Thomas et al. 1998; Colín, Klypin & Kravtsov 2000; Bullock 2002) and they exhibit a significant departure from spherical symmetry and isotropy. It is interesting to investigate if the response of a spherical subhalo to an imposed tidal field is the same as that of a triaxial subhalo.

KMM compared the resilience to tidal forces of two identical self-consistent NFW satellites on the same external tidal field and orbit, but constructed with different velocity dispersion tensors. Identifying the bound mass as function of time, these authors demonstrated that the satellite with a radially anisotropic velocity dispersion (Osipkov 1979; Merritt 1985) experiences much more efficient mass loss than its isotropic counterpart. This is due to the fact that particles on more radial orbits spend on average more time at larger radii and are therefore more easily stripped by the external field. Here we expand on the previous result and show that similar differences are obtained when one considers the tidal evolution of spherical and triaxial haloes as they orbit within a deeper potential. We compare results of the 3:1 prolate and oblate haloes and the initial isotropic spherical halo used to create these models. The density profile of the spherical model is scaled by a factor of four in mass to preserve the same spherically averaged density profile as the prolate halo. Each halo is then placed on an identical orbit within a static cored isothermal potential such that the ratio of host to satellite halo circular velocities is  $v_{\text{host}}/v_{\text{sat}} = 10:1$  and the apocentric to pericentric radii is  $r_{\text{apo}}/r_{\text{per}} = 4:1$ . The alignment of the axes of the triaxial satellite were varied with respect to the external deeper potential and the satellites always begin at the apocentre which is set equal to the virial radius. This allows the satellite-host system to be rescaled to any galactic or cluster system. The imposed potential is reasonably soft since we use a core radius equal to half the pericentric radius. Significantly higher rates of mass loss may be expected in a more cuspy potential, however

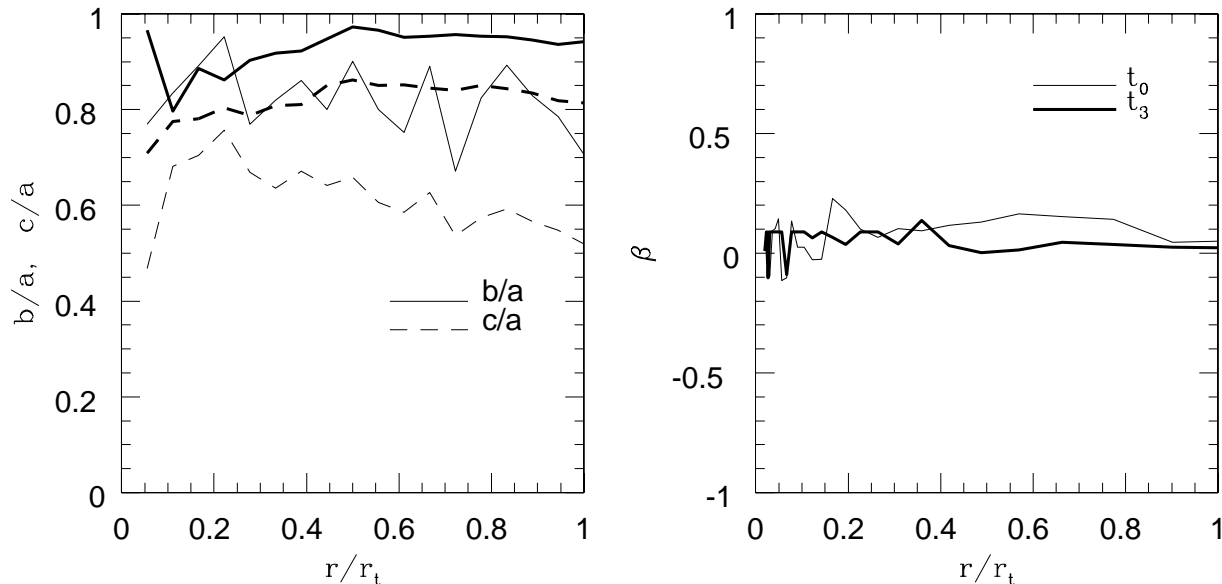


**Figure 8.** Structural and kinematic properties of one subhalo in our highest-resolution cosmological run (R12) resolved with more than  $2 \times 10^5$  particles. Left: The axial ratios  $b/a$  and  $c/a$  as a function of radius from the centre of the subhalo. Right: The anisotropy parameter  $\beta$  as a function of radius. In both cases, the thin lines correspond to measurements of the subhalo’s properties just before entering the primary halo, whereas the thick lines correspond to its third pericentric passage. The subhalo becomes more spherical and isotropic as a result of the tides. Note that the radius of the subhalo is given in units of  $r_t$ , where  $r_t$  is its tidal radius after the third pericentre passage.

here we aim to explore the slow tidal loss of mass rather than mass loss due to strong tidal shocks. In a forthcoming paper we will give an analytical model for the rate of mass loss as a function of host potential, orbit and subhalo structure and shape (Kazantzidis et al., in preparation).

In Figure 5 we perform a comparison of the tidal evolution of each of these three models by identifying the bound mass as a function of time using the publicly available group finder SKID<sup>1</sup> (Stadel 2001). The prolate halo experiences mass loss at a much higher rate than both the spherical and oblate ones. We also found that this result is not significantly sensitive to the alignment between the major or minor axis of the satellite and the orbital plane with the maximum differences in the mass loss being of the order of 25%. In Figures 6 and 7 we show the change in the shape and in the anisotropy parameter  $\beta$  of our models. We suspect that the prolate halo becomes more spherical due to the tidal removal of particles on radial orbits that are supporting the shape of the system. Future studies will analyse the orbital evolution of particles within the satellite to study these effects in detail. In addition, after 5 Gyr of orbital evolution the velocity dispersion tensor of the prolate halo has significantly changed and now is nearly isotropic.

It is interesting to study the evolution of shape and anisotropy for haloes in a CDM simulation that enter into a deeper potential. This is important when we want to model the orbits of stars in satellite galaxies or the effect of subhaloes on lense models. Here we analyse subhaloes from a high resolution  $\Lambda$ CDM cluster simulation (Diemand et al. 2004). The initial conditions are generated with the GRAFIC2 package (Bertschinger 2001). We start with a  $300^3$  particle cubic grid with a comoving cube size of 300 Mpc (particle mass  $m_p = 2.6 \times 10^{10} h^{-1} M_\odot$ ). We trace back and refine a cluster region by a factor of 12 in length and 1728 in mass, so that the mass resolution is  $m_p = 1.5 \times 10^7 h^{-1} M_\odot$ . The soft-

ening length is comoving from the start of the simulation ( $z \simeq 40$ ) to  $z = 9$ . From  $z = 9$  until present, we use a physical softening length of  $1.05 \times 10^{-3} r_{\text{vir,parent}}$ . At  $z = 0$  the refined cluster contains  $1.4 \times 10^7$  particles (R12) and we select a relatively massive subhalo which is resolved with more than  $2 \times 10^5$  particles.

Figure 8 shows the axial ratios  $b/a$  and  $c/a$  (left panel) and the anisotropy parameter  $\beta$  (right panel) as a function of radius for this object. The thin lines correspond to the subhalo just before entering its host, whereas the thick lines correspond to the third pericentre passage of the subhalo. Note that the radius of the subhalo is given in units of  $r_t$ , where  $r_t$  is its tidal radius after the third pericentre passage. Figure 8 confirms that subhaloes become more spherical and their velocity distribution more isotropic owing to tidal effects. We then compare the mean axial ratios of field haloes versus subhaloes in the same simulation. On average we find that subhaloes have axial ratios that are 30% larger (more spherical) than field haloes.

## 4 CONCLUSIONS

We have presented a method for constructing cuspy axisymmetric and triaxial  $N$ -body haloes based on merging isotropic equilibrium spherical haloes with varying amounts of angular momentum. In particular, we found that radial mergers produce prolate systems, while mergers on circular orbits produce oblate systems. This technique has the benefit that it is based on the way in which haloes obtain their triaxiality in cosmological simulations, therefore the anisotropy distributions and angular momentum of haloes are well motivated.

Mergers between similar equilibrium spherical haloes at high resolution show that the resulting halo has the same density profile, independent of the angular momentum of the merger. This has two implications: (i) the density profile of the triaxial halo can be set by the choice of the density profiles of the progenitor haloes

<sup>1</sup> <http://www-hpcc.astro.washington.edu/tools/skid.html>

and (ii) similar mass mergers can not dramatically re-arrange the central density structure of DM haloes, albeit oblate haloes (high angular momentum merger remnants) have concentrations up to a factor of two lower than prolate haloes (low angular momentum merger remnants). This may explain the entire scatter in the distribution of halo concentrations from cosmological simulations (Bullock et al. 2001; Eke et al. 2001; Wechsler et al. 2002). It may also be the case that the least concentrated haloes host the low surface brightness discs since these galaxies may form in high angular momentum oblate haloes (e.g., O’Neill et al. 1997). These galaxies generally require low values of the concentration when fit to cuspy halo models (e.g., McGaugh & de Blok 1998; van den Bosch et al. 2000; de Blok et al. 2001; Swaters et al. 2003).

As an application we considered the tidal evolution of triaxial subhaloes orbiting within deeper potentials. Haloes with identical spherically averaged density profiles and on identical orbits evolve self-similarly with time. Spherical haloes with isotropic velocity dispersion tensors suffer significantly less mass loss than radially anisotropic prolate ones. This is likely due to the fact that particles on radial orbits are easily stripped which also results in subhaloes becoming more spherical. In general, the subhaloes become more spherical and their velocity distribution more isotropic owing to tidal effects. This result has been confirmed by investigating the response to tides of both isolated satellite haloes orbiting within a static host potential and substructure haloes in the time dependent cosmological tidal field. We find that subhaloes in a cosmological simulation of a cluster are on average 30% rounder than their field counterparts. Galaxy subhaloes should be even closer to spherical since they spend longer being reshaped by the host potential.

Our more realistic modelling of DM haloes is important for studies of the weak and strong lensing statistics attempting to distinguish between competing cosmological models, the structural evolution and mass loss from substructure, the formation of tidal streams or the sizes of satellite haloes in galaxies and clusters. These results may also be important to incorporate within semi-analytic models that attempt to model the distribution of satellites in DM haloes. CDM haloes are generally radially anisotropic therefore they lose mass and are disrupted more quickly than the isotropic systems that have been generically considered in previous studies. This may explain why semi-analytic models predict far more substructures than found in high resolution numerical studies (e.g., Zentner & Bullock 2003, James Taylor private communication).

## ACKNOWLEDGMENTS

It is a pleasure to thank the anonymous referee for constructive comments on the manuscript and Victor Debattista and Lucio Mayer for useful discussions. BM thanks Priyamvada Natarajan for organising the Yale Cosmology Workshop “The Shapes of Galaxies and Their Dark Matter Haloes” (2001) which motivated some of this work and also apologises for not writing up the conference proceedings. The numerical simulations were carried out on the zBox (<http://www-theorie.physik.unizh.ch/~stadel/>). Initial conditions for the cosmological simulations were generated at the Swiss Center for Scientific Computing (SCSC) at Manno.

## REFERENCES

Barnes J. E., Efstathiou G., 1987, *ApJ*, 319, 575

Barnes, J. E. 1999, in IAU Symp. 186, *Galaxy Interactions at Low and High Redshift*, ed. J. E. Barnes & D. B. Sanders (Dordrecht: Kluwer), 137  
 Barnes, J. E. 1992, *ApJ*, 393, 484  
 Barnes, J. E., Hernquist, L. 1996, *ApJ*, 471, 115  
 Bartelmann M., Steinmetz M., Weiss, A., 1995, *A&A*, 297, 1  
 Bertschinger E., 2001, *ApJS*, 137, 1  
 Boily C. M., Kroupa P., Peñarrubia-Garrido J., 2001, *NewA*, 6, 27  
 Boylan-Kolchin M., Ma, C.-P., 2004, *MNRAS*, 349, 1117  
 Bullock J. S., Kolatt T. S., Sigad Y., Somerville R. S., Kravtsov A. V., Klypin A. A., Primack J. R., Dekel, A., 2001, *MNRAS*, 321, 559  
 Bullock J. S., 2002, in *The Shapes of Galaxies and Their Dark Haloes*, ed. P. Natarajan (Singapore: World Scientific), p. 109  
 Buote D. A., Canizares C. R., 1994, *ApJ*, 427, 86  
 Buote D. A., Canizares C. R., 1996, *ApJ*, 457, 177  
 Buote D. A., Canizares C. R., 1998, in *ASP Conf. Ser. 136, Galactic Haloes*, ed. D. Zaritsky (San Francisco: ASP), p. 289  
 Buote D. A., Jeltema T. E., Canizares C. R., Garmire G. P., 2002, *ApJ*, 577, 183  
 Cole S., Lacey, C., 1996, *MNRAS*, 281, 716  
 Colín P., Klypin A. A., Kravtsov A. V., 2000, *ApJ*, 539, 561  
 de Blok W. J. G., McGaugh S. S., Bosma A., Rubin, V. C., 2001, *ApJ*, 552, L23  
 Diemand J., Moore B., Stadel J. 2004, *MNRAS*, 352, 535  
 Dubinski J., Carlberg R.G., 1991, *ApJ*, 378, 496  
 Dubinski, J., 1998, *ApJ*, 502, 141  
 Eddington A. S., 1916, *MNRAS*, 76, 572  
 Eke V. R., Navarro J. F., Steinmetz M., 2001, *ApJ*, 554, 114  
 Franx M., van Gorkom J. H., de Zeeuw, T., 1994, *ApJ*, 436, 642  
 Frenk C. S., White S. D. M., Davis M., Efstathiou G., 1988, *ApJ*, 327, 507  
 Fulton, E., Barnes, J. E. 2001, *Ap&SS*, 276, 851  
 Gerhard, O. E. 1981, *MNRAS*, 197, 179  
 Hayashi E., Navarro J. F., Taylor J. E., Stadel J., Quinn T., 2003, *ApJ*, 584, 541  
 Hernquist L., 1990, *ApJ*, 356, 359  
 Hernquist L., 1993, *ApJS*, 86, 389  
 Holley-Bockelmann K., Mihos J. C., Sigurdsson S., Hernquist L., 2001, *ApJ*, 549, 862  
 Holley-Bockelmann K., Weinberg M., Katz N., 2003, submitted to *MNRAS* (astro-ph/0306374 )  
 Ibata R., Lewis G. F., Irwin M., Totten E., Quinn T., 2001, *ApJ*, 551, 294  
 Iodice E., Arnaboldi M., Bournaud F., Combes F., Sparke L. S., van Driel W., Capaccioli M., 2003, *ApJ*, 585, 730  
 Jing Y. P., Suto Y., 2002, *ApJ*, 574, 538  
 Johnston K. V., Zhao H., Spergel D. N., Hernquist L., 1999, *ApJ*, 512, L109  
 Kazantzidis S., Magorrian J., Moore B., 2004a, *ApJ*, 601, 37  
 Kazantzidis S., Kravtsov A. V., Zentner A. R., Allgood B., Nagai D., Moore B., 2004b, *ApJL*, 611, L73  
 Khochfar S., Burkert A., 2003, *MNRAS* submitted (astro-ph/0309611)  
 Kochanek C.S., 1995, *ApJ*, 445, 559  
 Koopmans L. V. E., de Bruyn A. G., Jackson N., 1998, *MNRAS*, 295, 534  
 Kuijken K., Tremaine S., 1994, *ApJ*, 421, 178  
 Lemson G., Kauffmann G., 1999, *MNRAS*, 302, 111  
 Majewski S., Skrutskie M.F, Weinberg M.D., Ostheimer J.C., 2004, *ApJ*, 599, 1082

- Mayer L., Moore B., Quinn T., Governato F., Stadel, J., 2002, MNRAS, 336, 119
- McGaugh S. S., de Blok W. J. G., 1998, ApJ, 499, 41
- Merrifield M. R., 2002, in *The Shapes of Galaxies and Their Dark Haloes*, ed. P. Natarajan (Singapore: World Scientific), p. 170
- Merritt D., 1985, AJ, 90, 1027
- Merritt D., Fridman T. 1996, ApJ, 460, 136
- Moore B., Calcáneo-Roldán C., Stadel J., Quinn T., Lake G., Sebastianiano G., Governato F., 2001, Phys. Rev. D, 64, 063508
- Naab, T., Burkert, A., 2003, ApJ, 597, 893
- Navarro J. F., Frenk C. S., White S. D. M., 1996, ApJ, 462, 563
- O’Neill K., Bothun, G., Cornell M. 1997, AJ, 113, 1212
- Oguri M., Lee J., Suto Y., 2003, ApJ, 599, 7
- Osipkov L. P., 1979, Soviet Astron. Lett., 5, 42
- Poon M. Y., Merritt D. 2001, ApJ, 549, 192
- Sackett P. D., Sparke L. S., 1990, ApJ, 361, 408
- Schoenmakers R. H. M., Franx M., de Zeeuw P. T., 1997, MNRAS, 292, 349
- Schwarzschild M., 1979, ApJ, 232, 236
- Schwarzschild M., 1993, ApJ, 409, 563
- Schweizer F., Whitmore B. C., Rubin V. C. 1983, AJ, 88, 909
- Sparke L. S., 2002, in *The Shapes of Galaxies and Their Dark Haloes*, ed. P. Natarajan (Singapore: World Scientific), p. 178
- Stadel J., 2001, PhD thesis, Univ. Washington
- Swaters R. A., Madore B. F., van den Bosch F. C., Balcells, M., 2003, ApJ, 583, 732
- Taffoni G., Mayer L., Colpi M., Governato F. 2003, MNRAS, 341, 434
- Terzić, B., 2003, submitted to MNRAS (astro-ph/0305005)
- Thomas P. A. et al. , 1998, MNRAS, 296, 1061
- Tinker J. L., Ryden B. S., 2002, submitted to ApJ (astro-ph/0209165)
- van den Bosch F. C., Robertson B. E., Dalcanton J. J., de Blok W. J. G., 2000, AJ, 119, 1579
- Villumsen, J. V., 1983, MNRAS, 204, 219
- Vitvitska M., Klypin A. A., Kravtsov A. V., Wechsler R. H., Primack J. R., Bullock J. S., 2002, ApJ, 581, 799
- Warren M. S., Quinn P. J., Salmon J. K., Zurek W. H., 1992, ApJ, 399, 405
- Wechsler R. H., Bullock J. S., Primack J. R., Kravtsov A. V., Dekel A., 2002, ApJ, 568, 52
- Weil, M. L., Hernquist, L. 1996, ApJ, 460, 101
- White, S. D. M., 1978, MNRAS, 184, 185
- Zentner A. R., Bullock J. S., 2003, ApJ, 598, 49

This paper has been typeset from a  $\text{\TeX}$ / $\text{\LaTeX}$  file prepared by the author.